

# SPOT-5/HRS STEREO IMAGES ORIENTATION AND AUTOMATED DSM GENERATION

Daniela Poli, Zhang Li, Armin Gruen

Institute of Geodesy and Photogrammetry, ETH Zurich, 8093 Zurich, Switzerland

## TS HRS(2) - DEM Generation from SPOT-5 HRS Data

**KEY WORDS:** SPOT, Pushbroom, Sensor model, Orientation, Matching, DEM

### ABSTRACT

HRS (High Resolution Sensor), carried on SPOT-5, is the first high-resolution sensor on the SPOT constellation that enables the acquisition of stereo images in pushbroom mode from two different directions along the trajectory. The Institute of Geodesy and Photogrammetry (IGP) participated as Co-Investor in the ISPRS-CNES initiative for the investigation on DEM generation from SPOT-5/HRS stereoscenes. This paper describes the work carried out at IGP on a stereopair acquired on 1st October 2002 over parts of Bavaria and Austria.

For orienting HRS imagery, two alternative approaches have been used: a rigorous sensor model and a rational function model. Both algorithms have been implemented at our Institute. The rigorous sensor model is based on the classical collinearity equations, which are extended by the sensor external orientation modeling with 2nd order piecewise polynomials depending on time and by self-calibration parameters. Using well distributed Ground Control Points (GCPs), the unknown internal and external parameters are estimated with a least squares solution. The alternative method, independent from the camera model, does not describe the physical imaging process, but uses rational polynomials to relate image and ground coordinates to each other. This algorithm consists of two steps: 1) calculation of Rational Polynomial Coefficients (RPC) for each image with a least-squares using the geometric information contained in the metadata files; 2) block adjustment with the computed RPC model using GCPs. Both orientation methods gave RMS errors in Check Points (CPs) in the range of 1 pixel in all coordinate directions.

Using the triangulated orientation elements, the DSM was extracted with algorithms and software packages for CCD linear sensors developed at IGP. After the creation of image pyramids, the matches of three kinds of features (feature points, grid points and edges) on the original images are found progressively in the next levels starting from the low-density features on the images with the lowest resolution. A triangular irregular network based DSM is constructed from the matched points on each level of the pyramid and used in turn in the subsequent pyramid level for the approximations and adaptive computation of the matching parameters. A modified Multi Photo Geometrically Constrained Matching algorithm is employed in order to achieve sub-pixel accuracy for all the matched features. The extracted DSM was compared to the reference DSMs obtained from laser data and map contours at different spacings (5x5 m, 25x25 m and 50x50 m) provided by DLR in Oberpfaffenhofen using both terrain height and orthogonal distances. The results show RMS values between one and two pixels on the average and a systematic error mainly due to the presence of trees. After a manual removal of the main areas covered by trees in the reference DSMs sites those errors have been removed. The final results show a mean error in the range of 1-5 meters.

## 1. INTRODUCTION

SPOT-5 was launched on 4<sup>th</sup> May, 2002 by Arianespace from the Kourou Space Centre in French Guyana. After completing two months of in-orbit tests it became fully operational in July 2002.

SPOT-5 belongs to the SPOT (Satellite Pour l'Observation de la Terre) constellation developed by CNES (Centre National D'Etudes Spatiales). The constellation consists of 3 operational satellites (SPOT-2, SPOT-4 and SPOT-5) flying along a near-polar, near-circular and Sun-synchronous orbit at a mean altitude of 832 km, an inclination of 98.7 degrees and a mean revolution period equal to 101.4 minutes. The SPOT satellites orbit the same ground track every 26 days with a nominal cycle of 369 revolutions and cross the equator from North to South at 10:30 a.m. mean local solar time (Gleyzes et al., 2003).

Within the constellation, SPOT-5 is the most innovative satellite. The new HRG (High Resolution Geometry) instruments, derived from the HRVIR instrument on SPOT-4 offer high resolution in across-track direction with up to 2.5m resolution in panchromatic mode. Moreover the new HRS (High Resolution Sensor) allows the acquisition of stereo images in along-track direction, using two telescopes pointing about 20 degrees forward and backward (Gleyzes et al., 2003).

Other payload packages include the same Vegetation instrument as on SPOT-4, and the DORIS instrument, for greater orbital accuracy.

The Institute of Geodesy and Photogrammetry (IGP) of ETH Zurich joined the HRS Scientific Assessment Program (HRS-SAP), organised by CNES and ISPRS. This initiative, announced in Denver in 2002 at the ISPRS Commission I Symposium, has the aim to investigate the potential of SPOT-5/HRS sensor for DEM generation in order to help CNES to improve its future Earth Observation systems and all users to better know and trust the accuracy and quality of the HRS instrument and the derived DEM (Baudoin et al., 2003).

IGP joined the Initiative as Co-Investigator, that is, it processed the data provided by one the Principal Investigators, generated two DEMs with two different orientation methods, compared them to the reference DEMs and produced a quality report.

In this paper the work carried out at IGP within HRS-SAP is reported. After the description of the available data, the processing algorithms applied for images orientation, matching and DEM generation are presented. The results obtained after the comparison between the generated DEMs with the reference ones are reported and analysed. Final comments will conclude the paper.

## 2. DATA

Within the Initiative, CNES and DLR Oberpfaffenhofen provided the data set number 9 (Chiemsee), consisting of:

- two stereo images from SPOT5-HRS sensor with corresponding metadata files;
- the description of the exact position of 81 object points in Germany, measured with surveying methods;
- reference DEMs produced by Laser data and conventional photogrammetric and geodetic methods.

In the next paragraphs the main data characteristics are reported.

### 2.1 SPOT-5/HRS scenes

The two stereo images were acquired on 1<sup>st</sup> October 2002 in the morning from 10:15 to 10:18 (forward) and from 10:18 to 10:21 (backward) over an area of approximately 120x60 km<sup>2</sup> in Bavaria and Austria.

Each image is 12000 x 12000 pixel large, with a ground resolution of 10m across and 5 m along the flight (parallax) direction. The scenes were acquired in panchromatic mode in stereo viewing along the flight direction with a base over height ratio of 0.8. The two telescopes contained in the HRS instrument scan the ground with off-nadir angles of +20 degrees (forward image) and -20 degrees (backward image). Each telescope has a 580 mm focal length and a focal plane with a CCD line of 12000 pixels, 6.5 μm size. The main sensor characteristics are reported in Table 1.

The scenes cover an area with flat, hilly and mountainous (Alps) terrain, agriculture areas, towns, rivers and lakes. The height ranges between 400 m and 2000 m. Clouds are absent (Figure 2).

The metadata files contain information on the acquisition time and image location, ephemeris (sensor position and velocity from GPS at 30 seconds time interval, attitude and angular speeds from star trackers and gyros at 12.5 seconds interval), sensor geometric (detectors looking angles) and radiometric calibration. For a detailed description of the metadata file see DIMAP site. The on-board determination of the satellite position and the absolute dating are supplied by DORIS (Doppler Orbitography and Radiopositioning Integrated by Satellite).

DORIS is a one-way microwave tracking system developed for precise orbit determination (1m RMSE) by GRGS (Groupe de Recherches de Géodésie Spatiale) and IGN (Institut Géographique National). The concept is based on a ground segment (of globally positioned tracking stations) and a space segment (i.e. DORIS as a passenger payload in a satellite consisting of a receiver, an ultra-stable oscillator and an antenna). There is also a control centre as part of the ground segment, located at CNES (Gleyzes et al., 2003). The onboard receiver measures the Doppler shift of uplink beacons in two frequencies ( $f_1 = 2036.25$  MHz,  $f_2 = 401.25$  MHz), which are transmitted continuously by the DORIS ground network of stations. One measurement is used to determine the radial velocity between spacecraft and beacon, the other to eliminate errors due to ionosphere propagation delays.

Table 1. SPOT5-HRS characteristics (Source CNES).

Mass	90 kg
Power	128W
Dimensions	1 x 1.3 x 0.4 m
Field of view	8°
Focal length	0.580 m
Detectors per line	12,000
Detector pitch	6.5 μm
Integration time per line	0.752 ms
Off-nadir angles:	
-forward	20°
-backward	-20°
Spectral range (PAN)	0.49 μm - 0.69 μm
Ground sample distance:	
-across track	10 m
-along track	5 m
Modulation transfer	> 0.25 function
Signal-to-noise ratio	> 120

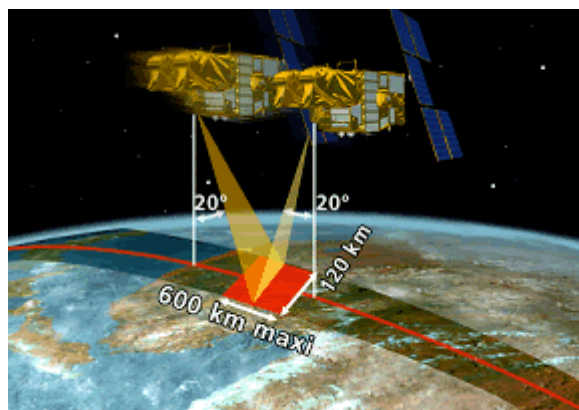


Figure 1. SPOT-5/HRS along-track image acquisition (Source: CNES).

### 2.2 Reference DEMs

The reference DEMs provided by DLR Oberpfaffenhofen are:

- 4 DEMs in southern Bavaria (Prien, Gars, Peterskirchen, Taching) created from Laser scanner data with a point spacing of 5 meters and an overall size of about 5 km x 5 km. The height accuracy is better than 0.5 m;
- 1 DEM (area of Inzell, total: 10 km x 10 km, 25 m spacing) partly derived from laser scanner data (northern part, height accuracy better than 0.5 m) and partly derived from contour lines 1:10 000 (southern part, height accuracy of about 5 m);
- A large coarse DEM (area of Vilsbiburg, 50 km x 30 km) with 50 m spacing and a height accuracy of about 2 meters, derived by conventional photogrammetric and geodetic methods.

In Table 2 the principal characteristics of the reference DEMs are summarised.

Table 2. Main characteristics of reference DEMs.

DEM	Location	Terrain characteristics	DEM Spacing (m)	Source	DEM Size (kmxkm)	Height Accuracy (m)
1	Prien	Smooth, weakly inclined	5x5	Laser Scanner	5x5	0.5
2	Gars	Smooth, weakly inclined	5x5	Laser Scanner	5x5	0.5
3	Peterskirchen	Smooth, weakly inclined	5x5	Laser Scanner	5x5	0.5
4	Taching	Smooth, weakly inclined	5x5	Laser Scanner	5x5	0.5
5-1	Inzell-North	Rough, strongly inclined	25x25	Laser Scanner	10x1.3	0.5
5-2	Inzell-South	Rolling, strongly inclined	25x25	Contour lines	10x7.7	5.0
6	Vilsbiburg	Rough, weakly inclined	50x50	Photogrammetry	50x30	2.0

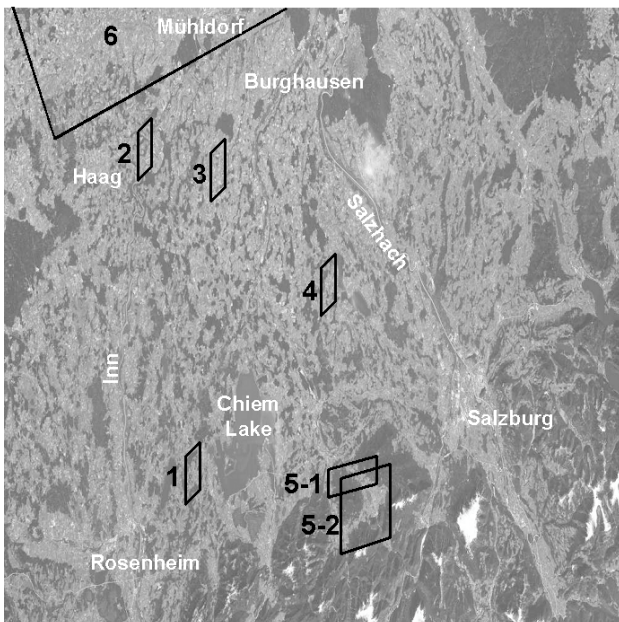


Figure 2. SPOT-5/HRS forward scene with some topographic elements in white (towns, rivers and lakes) and location of reference DEMs (in black) with same notation used in Table 2.

### 3. POINT MEASUREMENTS

From the available 81 object points, only 41 have been identified in the images. In order to locate them in the images a digital map at 1:50,000 scale (Topo50) was used. The coordinates were given in the Gauss-Krueger system. The exact image coordinates of the points have been measured with unconstrained Least Squares Matching developed at IGP (Baltasvias, 1991), by measuring the points in the master image manually. The final point distribution is shown in Figure 3.

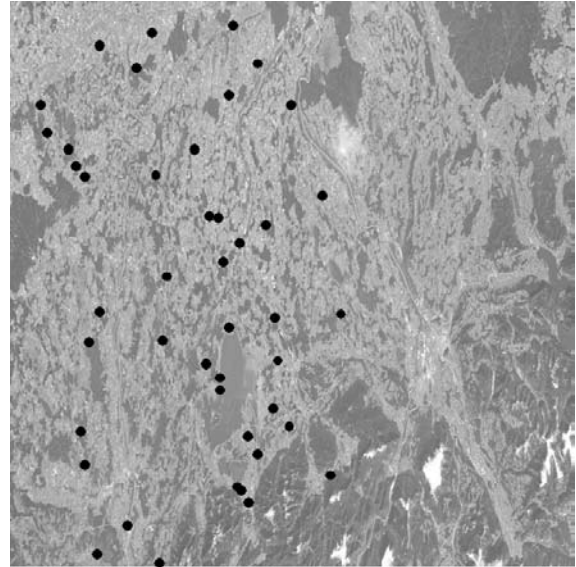


Figure 3. Distribution of 41 object points (in black).

### 4. IMAGES ORIENTATION

The HRS (High-Resolution Stereoscopic) instrument of SPOT-5 uses linear arrays that scan a single image line at an instant of time in the so-called pushbroom mode. Consequently each line of the HRS image is acquired at a different exposure station with different orientation elements. For the orientation of this kind of imagery two approaches, based on rigorous models and rational function models, are used.

The rigorous model tries to describe the physical properties of the sensor and its image acquisition mode. It is based on collinearity equations, which are extended in order to describe the specific geometry of pushbroom sensors. The adjustment parameters must include the exterior orientation and self-calibration parameters to describe the physical imaging process. Alternatively, rational function models use a general transformation to describe the relationship between image and ground coordinates.

In this work both approaches have been applied. In the next paragraph the algorithms used for the orientation will be described and the results reported.

#### 4.1 Procedure 1: Rigorous model

The aim of rigorous sensor models is to establish a relationship between image and ground reference systems according to the sensor geometry and the available data. For the georeferencing of imagery acquired by pushbroom sensors many different geometric models of varying complexity, rigor and accuracy have been developed, as described in (Fritsch et al., 2000) and (Dowman et al., 2003). A flexible sensor model for the georeferencing of a wide class of linear CCD array sensors has been developed at IGP and already applied to different linear

scanners carried on satellite and aircraft (Poli, 2003). The model is based on the photogrammetric collinearity equations, because each image line is the result of a nearly parallel projection in the flight direction and a perspective projection in the CCD line direction.

The model can be applied to single- and multi-lens sensors. In case of multi-lens sensors, like SPOT-5/HRS, additional parameters describing the relative orientation (displacements and rotations) of each lens with respect to a suitable central point are introduced. During the georeferencing of images from linear CCD array scanners, particular attention must be paid to their external orientation, because each image line is acquired with a different external orientation, that cannot be estimated with a classical bundle adjustment, due to the large number of unknowns (6 for each image line). The sensor position and attitude are modeled with piecewise 2<sup>nd</sup> order polynomial functions depending on time. The platform trajectory is divided into segments according to the number and distribution of available Ground Control Points (GCPs) and Tie Points (TPs) and for each segment the sensor position and attitude are modeled by 2<sup>nd</sup> order polynomials. At the points of conjunction between adjacent segments constraints on the zero, first and second order continuity are imposed on the trajectory functions. Additional pseudo-observations can fix some or all parameters to suitable values. For example, if the 2<sup>nd</sup> order parameters are fixed to zero, the polynomial degree is reduced to 1 (linear functions). This option allows the modeling of the sensor position and attitude in each segment with 2<sup>nd</sup> or 1<sup>st</sup> order polynomials, according to the characteristics of the trajectory of the current case study. In case of sensors carried on aircraft, additional GPS and INS observations can be included in the model (Poli, 2002).

The sensor model includes also a self-calibration, which is required for the correction of the systematic errors due to: principal point displacement ( $d_x$ ,  $d_y$ ), focal length variation ( $d_c$ ), radial symmetric ( $k_1$ ,  $k_2$ ) and decentering lens distortion ( $p_1$ ,  $p_2$ ), scale variation in CCD line direction ( $s_y$ ) and the CCD line rotation in the focal plane ( $\theta$ ).

Finally the functions modeling the external and the internal orientation are integrated into the collinearity equations, resulting in an indirect georeferencing model. Due to their non-linearity, the complete equations are linearized according to the first-order Taylor decomposition with respect to the unknown parameters. For this operation initial approximations for the unknown parameters are needed. The resulting system is solved with a least squares method. An overview of this sensor model is given in Figure 4.

The sensor model was applied in order to orient the stereopair and estimate the ground coordinates of the Check Points (CPs). The available ephemeris (sensor position and velocity) were used to generate the approximate values for the parameters modeling the sensor external orientation (position and attitude) in fixed Earth-centred geocentric Cartesian system.

The GCPs coordinates were transformed into the same system. From the available 41 object points, a group of them was used as GCPs and the remaining as CPs. Different tests have been carried out in order to choose the best input configuration.

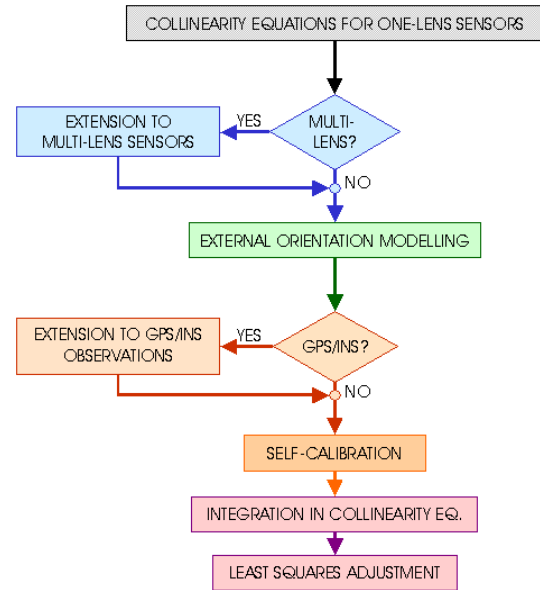


Figure 4. Flowchart with main components of the rigorous sensor model.

The tests were set as follows:

- external orientation modeling with quadratic functions, varying the number of segments and GCPs configurations, no self-calibration;
- external orientation modeling with linear and quadratic functions, best GCPs configuration and best trajectory segments, no self-calibration;
- self-calibration with best external orientation modeling configuration.

The choice of the unknown self-calibration parameters to include in the modeling is based on the analysis of the cross-correlation between the self-calibration parameters, the external orientation parameters and the ground coordinates of the TPs.

The best results in the CPs were obtained by modeling the external orientation with 2 segments and 2<sup>nd</sup> order functions and with self-calibration. The self-calibration parameters that mostly influenced the model were  $k_1$ ,  $k_2$ ,  $p_2$  and  $s_y$  for both lenses and  $\theta$  for both lines. The other self-calibration parameters were not used because they correlated highly (>95%) with the external orientation parameters. By changing the number of GCPs and TPs, the RMSE were always less than 1 pixel (Table 3). Figure 5 shows the residuals in planimetry (top) and in height (bottom) using all the object points as GCPs.

Table 3. RMSE for all points using rigorous orientation model.

Number of GCPs + CPs	RMSE in East (m)	RMSE in North (m)	RMSE in Height (m)
8 + 31	3.68	6.52	4.75
16 + 25	3.46	6.22	3.75
41 + 0	3.24	5.52	3.68

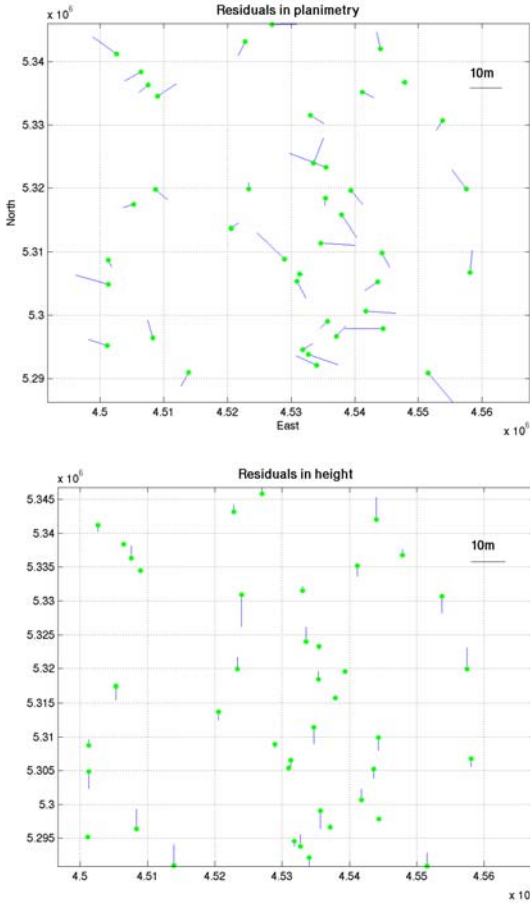


Figure 5. Residuals in planimetry (top) and height (bottom) for all 41 GCPs.

#### 4.2 Procedure 2: Rational functions model

The alternative approach is based on the RPC (Rational Polynomial Coefficients) model. The idea is to describe the camera model contained in the metadata file with suitable rational functions and apply a block adjustment to correct for remaining systematic errors (Zhang et al., 2004). The procedure consists of two main steps:

1. RPC model estimation. After generating a 3D grid of points using the given camera model parameters, the ephemeris and the attitude data attached in the metadata file, the RPC coefficients are determined by a least-squares approach and without GCPs. For details see (Tao et al., 2001). The Equations used for this are rational functions:

$$\begin{aligned} x &= RPC_x(\varphi, \lambda, h) = \frac{NUM_x(\varphi, \lambda, h)}{DEN_x(\varphi, \lambda, h)} \\ y &= RPC_y(\varphi, \lambda, h) = \frac{NUM_y(\varphi, \lambda, h)}{DEN_y(\varphi, \lambda, h)} \end{aligned} \quad (1)$$

Here  $(\varphi, \lambda, h)$  are normalised object-space geographic coordinates (latitude, longitude and height) and  $(x, y)$  are normalised image coordinates, in line and column direction.  $NUM_x$ ,  $NUM_y$ ,  $DEN_x$  and  $DEN_y$  are 3<sup>rd</sup> order polynomials on  $(\varphi, \lambda, h)$ , resulting in 67 unknown parameters for each image. The 3D grid of object points is generated from the image-space coordinates, for a set of elevation levels. The RPCs were computed for the whole

- test HRS scenes with an internal fitting accuracy of 0.07 pixels (RMSE) and 0.23 pixels maximum difference.
2. Block adjustment with computed RPC model. After the RPC generation in step 1, a block adjustment was performed in order to estimate 6 parameters for each image (affine transformation) to remove remaining systematic errors. As mathematical model of the adjustment, we used the method proposed by (Grodecki et al., 2003). The method is an affine transformation:
$$\begin{aligned} x + a_0 + a_1x + a_2y &= RPC_x(\varphi, \lambda, h) \\ y + b_0 + b_1x + b_2y &= RPC_y(\varphi, \lambda, h) \end{aligned} \quad (2)$$

where  $a_0, a_1, a_2$  and  $b_0, b_1, b_2$  are the adjustment parameters for an image,  $(x, y)$  and  $(\lambda, \varphi, h)$  are image and object coordinates of a GCP or a tie point.

Using this adjustment model, we expect that  $a_0$  and  $b_0$  will absorb any shifts and misalignments in the position and attitude, and the residual interior orientation errors in image line and sample directions. The parameters  $a_1, a_2, b_1, b_2$  are used to absorb the effects of on-board drift errors.

The adjustment results are shown in Table 4 and Figure 6.

Table 4. RMSE for all points with the RPC orientation method.

Number of GCPs + CPs	RMSE in East (m)	RMSE in North (m)	RMSE in Height (m)
4 + 37	5.28	3.87	2.64
8 + 33	5.63	3.96	2.38
41 + 0	4.63	3.66	2.21

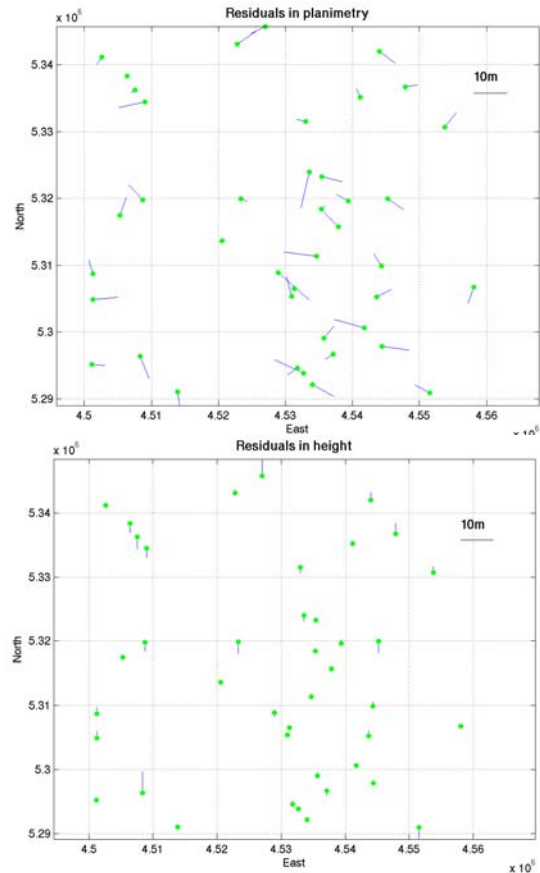


Figure 6. Results in planimetry (top) and height (bottom) from block adjustment with the RPC model and 41 GCPs.

## 5. MATCHING

In order to automatically extract the DTM / DSMs from the linear array images (airborne or spaceborne), algorithms and software package developed in our group (see Gruen et al., 2002 and Zhang et al., 2003) have been used.

The matching algorithm combines the matching results of the feature points, grid points and edges. It uses a modified version of the MPGC (Multi Photo Geometrically Constrained) matching algorithm (see Gruen, 1985, Gruen et al., 1988 and Baltasvias, 1991) and can achieve sub-pixel accuracy for all the matched features.

Figure 7 shows the workflow of our image matching procedure.

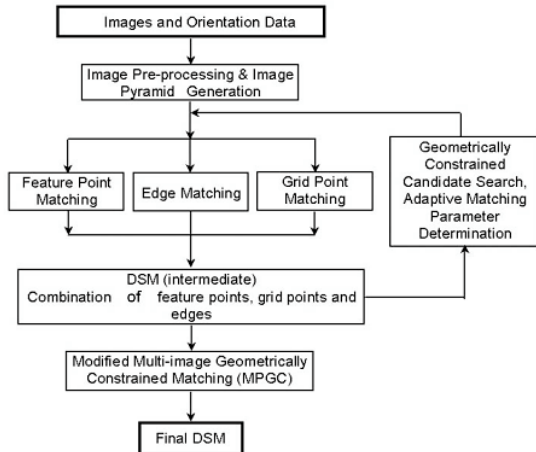


Figure 7. Workflow of the image matching procedure.

For the DSM/DEM generation, the SPOT-5/HRS images and the previously triangulated orientation elements were used. After the pre-processing of the imagery and production of the image pyramid, the matches of three kinds of features, i.e. feature points, grid points and edges, are found progressively in all pyramid levels starting from the low-density features on the images with the lowest resolution. A Triangular Irregular Network (TIN) based DSM is constructed from the matched features on each level of the pyramid and is used in turn in the subsequent pyramid level as approximation for the adaptive computation of the matching parameters. Finally the modified MPGC matching is used to achieve more precise results for all the matched features on the original resolution level (level 0) and to identify some inaccurate and possible false matches. The raster DTM / DSMs are interpolated from the original matching results.

The main features of this matching procedure are:

- It is a combination of feature point, edge and grid point matching. The grid point matching procedure uses relaxation-based relational matching algorithm and can bridge over the non- / little-texture areas through the local smoothness constraints. Edges are introduced to control the smoothness constraints in order to preserve the surface discontinuities.
- The matching parameters include the size of the matching window, the search distance and the threshold value for cross-correlation and MPGC (Least Squares matching). For instance, the procedure uses a smaller matching window, a larger search distance and a smaller threshold value in rougher terrain areas and vice versa. The roughness of the terrain is computed from the approximate DSM on the higher level of image pyramid. The adaptive determination of the matching parameters results in higher success rate and less false matches.

- Line features are important for preserving the surface discontinuities. For this reason a robust edge matching algorithm, which uses the adaptive matching window determination through the analysis of the image contents and local smoothness constraints along the edges, is combined into our procedure.
- Together with point features, edges (in 3D) are introduced as breaklines when a TIN-based DSM is constructed in order to provide good approximations for the matching on the next pyramid level. The computation of the approximate DSM for the highest-level image pyramid uses a matching algorithm based on the *region-growing* strategy (Otto et al., 1988). According to this approach the already measured GCPs and TPs are considered as *seed points*.
- The quality control procedure consists of (1) the local analysis of the smoothness and consistence of the intermediate DSM on each image pyramid level (2) the analysis of the difference between the intermediate DSMs and (3) the analysis of the MPGC results. Blunders can be detected and deleted.
- For each matched feature, a reliability indicator is assigned. Its value is based on the analysis of the matching statistics (cross-correlation and MPGC results). As a consequence, different weights are used during the generation of the grid-based DSM/DEM.

Considering the characteristics of the SPOT-5/HRS image data, some small modifications were introduced in our matching procedure:

- The HRS imagery has 10 meters resolution in cross-track direction and 5 meters in along-track direction (parallax direction). This configuration may result in better accuracy for point determination and DEM generation, but causes some difficulties during the (area-based) matching procedure. In order to avoid the problems, the images have been resampled from 10m x 5m to 10m x 10m and processed with our matching procedure (except the MPGC part). Then the MPGC (Least Squares matching) was run on the original images in order to recover the original matching accuracy. This two-step method results in the reduction of the search distance between corresponding points, which is equivalent to the reduction of the possibility of false matching and the processing time.
- In some difficult areas, like small and steep geomorphologic features (an example is shown in Figure 8), some manually measured points can be introduced as *seed points*. This operation gives better approximations for the matching.

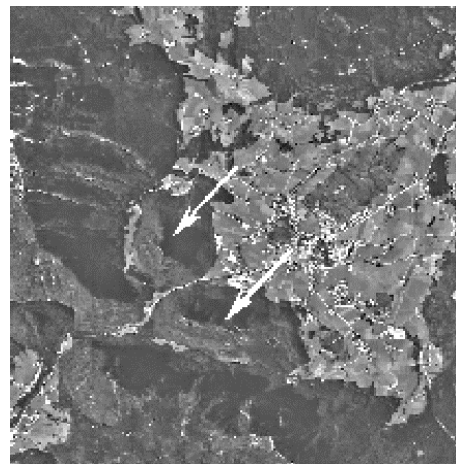


Figure 8. Manually measured seed points in difficult areas (two small hills with steep slopes).

## 6. DSM GENERATION

The test area includes a mountainous area (rolling and strongly inclined alpine area) on the South part and some hill areas (rough/smooth and weakly inclined areas) on the North part. In order to capture and model the terrain, our image matching software not only generates a large number of mass points (feature points and grid points) but also produces linear features. The TIN based DEM was generated from the matched mass points and the edges (as break-lines). An example of edge matching is shown in Figure 9. As can be seen in this Figure,

even in areas of steep mountains there are many successfully matched linear features. More than 8.4 million points have been matched and 80% of them are marked as 'reliable' points.

Some areas, as lakes and rivers, can be manually set as 'dead areas' with a user-friendly interface. In Figure 10 the 3D visualization of the generated DEM is shown. It can be seen that the shape of the DSMs is similar to the reference surfaces, but smoother. This can be expected from the limited resolution of the satellite images.

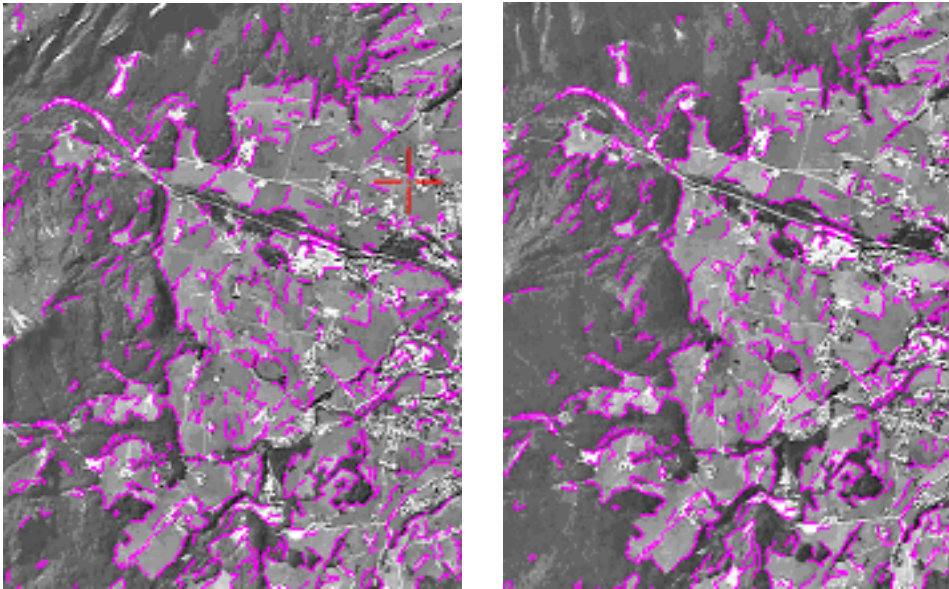


Figure 9. Image window overlapped with matched edges (in violet colour)

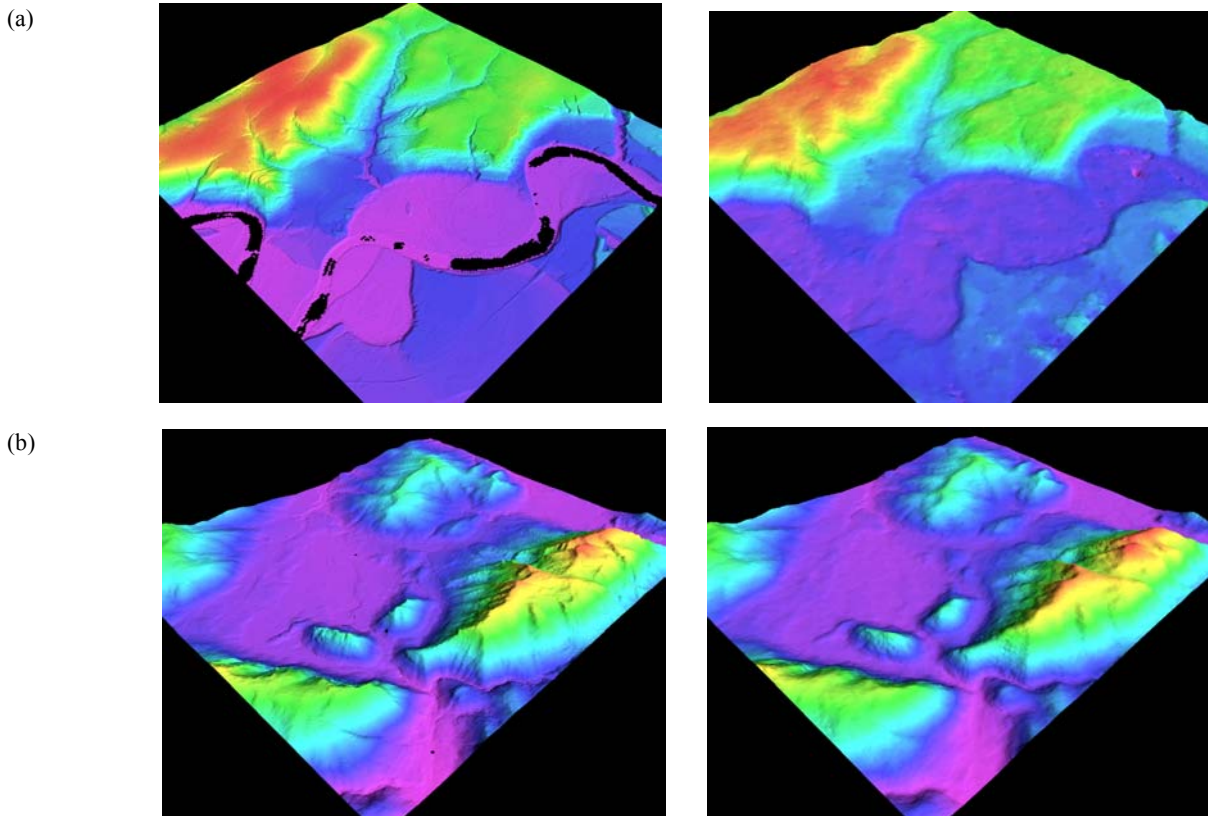


Figure 10. (a): 3D visualization of the reference DEM 2 (5m grid, on the left) and the generated DSM (15m grid, on the right); (b): 3D visualization of the reference DEM 5-2 (25m grid, on the left) and the generated DSM (25m grid, the right).

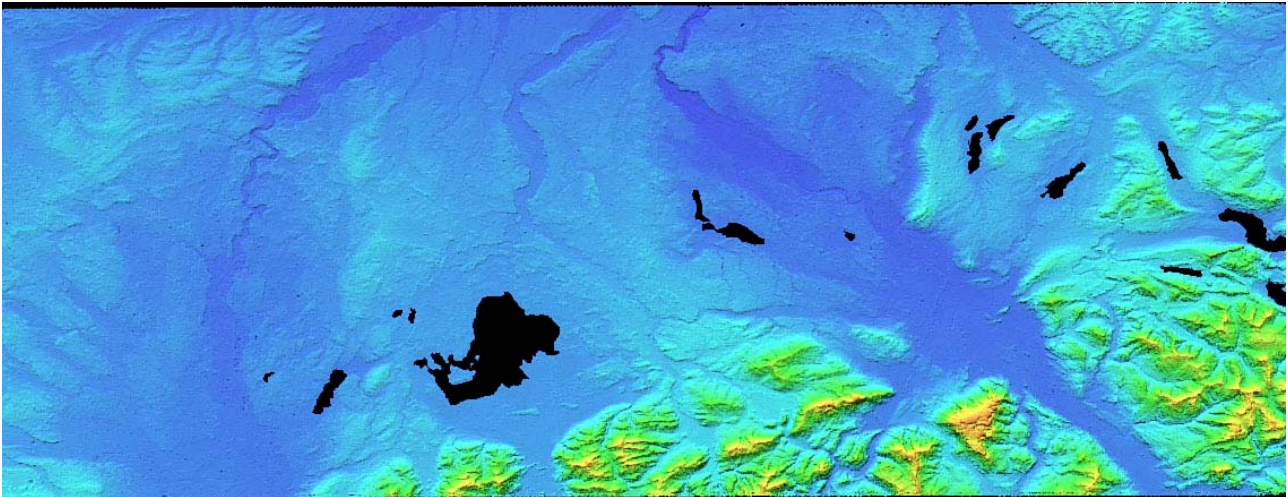


Figure 11. DEM generated for the whole are of 120km x 60km.

## 7. ACCURACY ANALYSIS

Two DSMs have been generated using the two orientation methods described in Section 4. These DSMs has been compared to the reference DEMs provided by the HRS-SAP. The main characteristics (location, spacing, source, size and height accuracy) of the reference data are shown in Table 2. The coordinate system used in the comparison is the Gauss-Krueger system, Zone 4, with Bessel ellipsoid and Potsdam datum.

Two accuracy tests have been performed in 2.5 D and 3D respectively. In the first test the differences between the heights of the reference DEMs and the corresponding height interpolated from our DSMs have been computed (2.5D). The limit of this approach is that it is highly influenced by the errors of the surface-modelling algorithm. Figure 12 illustrates the concept with a step profile: even if the measurements (green points) are accurate, the modeled profile can not follow the true one. Consequently if the terrain height is compared, in the correspondence of the step, a large difference ( $\Delta h$ ) may be measured. For that reason the computation of the 3D orthogonal distance between the surfaces (distance  $d$  in Figure 12) is theoretically more correct.

Therefore the second accuracy test is based on the evaluation of the normal distance (3D) between our measurements and the reference DEMs. This test is fundamental in this case study where steep mountains (Alps) are present.

The two tests have been made separately for each DEMs obtained by the procedures described in Section 4. The results are reported in the next paragraphs.

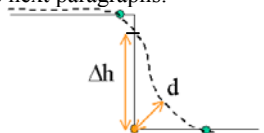


Figure 12. Modelling problems. The true profile is the full black line, the modelled profile is the dashed line.

### 7.1 Accuracy tests on the terrain height (2.5D)

The results obtained by this test are reported in Table 5. It can be observed that the accuracy of the generated DSM is more or less on 1.0 ñ 2.0 pixels level, depending on the terrain type. As expected, better accuracy are achieved in smooth and flat areas, while in the mountainous area (DEM 5-1 and 5-2) the RMSE are larger. In all datasets some blunders which failed to be

detected are still present. In the reference datasets called 5-1 and 5-2 some blunders are even above 100 meters, with bias up to 1.0 pixels. Apart from the results of reference DEM 6, all the biases are negative, indicating that our generated DSMs are higher than the reference ones. The results obtained by orientation Procedure 2 appear slightly better than the corresponding results achieved with Procedure 1. The differences between the two orientation approaches are in the order of quarter a pixel.

For further analysis, the frequency distribution of the height differences is shown in the second and third columns of Table 6. In the frequency distribution of the height differences two peaks occur, one located around value 0.0 and the other one around a negative value (ca. 8m). The relative frequency values are correlated to the percentage of presence of trees. In fact trees causes negative height difference (the green areas), while the open areas have small height difference values. It can be concluded that the bias located at ñ8m is mainly caused by the trees. This is a main problem for extracting DEM by using the optical imaging systems, as the light cannot penetrate the vegetation. For this reason the areas covered by trees have been manually removed from the images and the accuracy tests have been repeated. The percentage of removed points is 25, 26, 17, 28, 75 and 71 for DEM 1, 2, 3, 4, 5-1, 5-2 and 6 respectively. The results obtained by the new accuracy tests are shown in the last two columns of Table 5. As expected, the negative bias was reduced. This is also graphically confirmed by the new frequency distribution reported in the fourth columns of Table 5. The analysis of the frequency distributions shows that in steep mountain areas (DEM 5-1 and DEM 5-2) there are positive height-difference values. They are probably caused by the presence of blunders or by the local smoothness constraints used in our matching algorithm. These constraints smooth out some steep and small features of the mountain areas under the condition that there are not enough extracted and matched linear features.

### 7.2 Accuracy tests on the orthogonal distance between two 3D surfaces

This accuracy test has been carried out with the commercial software Gomatic Studio v.4.1 by Raindrop. This software calculates the normal distance between each triangle of a surface (in our case the reference DEMs) and the closest point

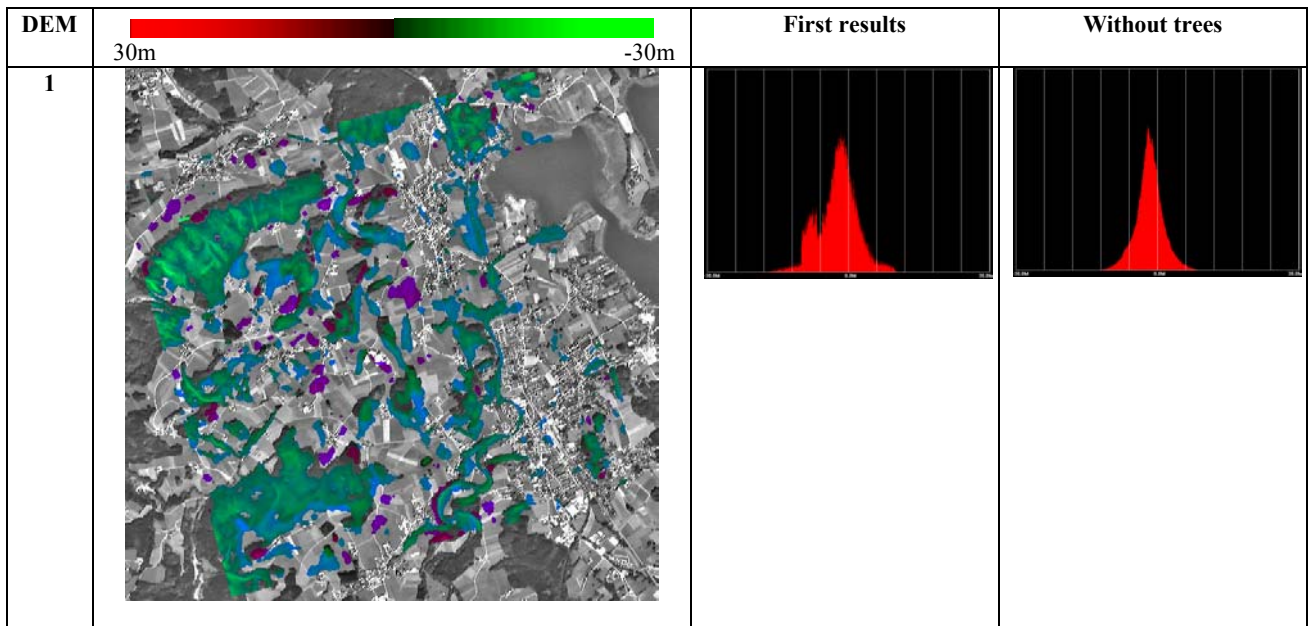
belonging to a point cloud (in our case, the two sets of measurements). The generated DEMs have been compared to the reference ones. The results are reported in Table 7. It can be seen a large reduction of the mean distance and standard deviation in all datasets. This demonstrates that part of the

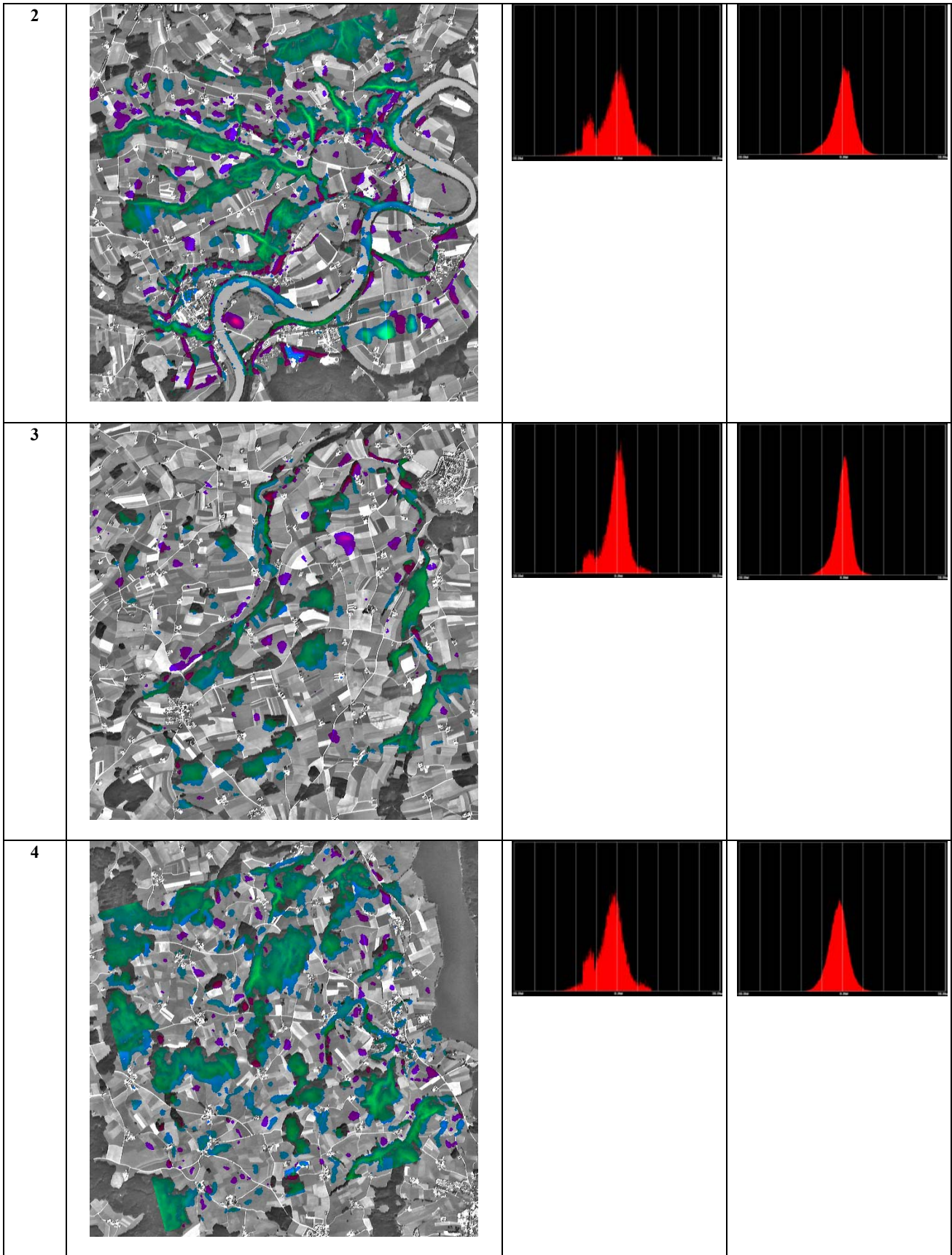
errors estimated with the 2.5D accuracy tests may be due to modelling errors or to the planimetric errors. Again, the larger errors have been found in mountainous areas (DEM 5-2), while in flat terrains the accuracy of the generated DEMs is very good. The two orientation procedures give very similar results.

Table 5. Accuracy results using 2.5D comparisons. All results are in meters.

DEM	Number of points		All points Procedure 1				All points Procedure 2				Without trees Procedure 1				Without trees Procedure 2			
	IGP DEM	Reference DEM	Max Diff.	Min Diff.	Mean	RMSE	Max Diff.	Min Diff.	Mean	RMSE	Max Diff.	Min Diff.	Mean	RMSE	Max Diff.	Min Diff.	Mean	RMSE
1	35448	1000000	22.1	-26.1	-4.0	6.2	25.1	-32.9	-2.6	5.7	13.8	-23.6	-3.0	5.4	15.4	-23.7	-1.7	4.6
2	32932	1000000	37.7	-37.1	-3.0	5.5	29.1	-37.1	-1.2	5.0	32.3	-31.2	-1.8	3.9	29.1	-31.7	0.2	3.6
3	33450	1000000	19.7	-17.8	-1.9	4.0	20.7	-17.2	-0.5	3.2	19.6	-14.1	-2.3	3.4	20.7	-13.6	0.1	2.9
4	32067	1000000	11.5	-21.7	-3.8	5.2	13.6	-23.1	-2.5	4.7	9.5	-17.1	-2.8	3.9	10.5	-18.4	-1.2	3.2
5-1	10327	21200	27.1	-36.8	-6.7	9.4	19.2	-33.5	-5.8	8.3	16.1	-23.3	-3.4	5.3	19.1	-13.3	-1.7	4.9
5-2	71795	139200	130.3	-86.1	-5.7	11.2	136.8	-89.3	-4.3	9.5	104.7	-55.5	-4.0	7.4	49.8	-66.8	-1.3	6.7
6	130558	600000	22.7	-19.0	1.1	3.8	26.8	-27.1	1.5	4.0	21.9	-14.6	-0.7	3.9	26.8	-25.9	2.1	4.4

Table 6. Accuracy analysis based on terrain heights. First column: name of reference dataset. Second column: 2D distribution of the height differences. Third column: Frequency distribution of the height differences of all points. Forth column: frequency distribution of the height differences without the tree areas.





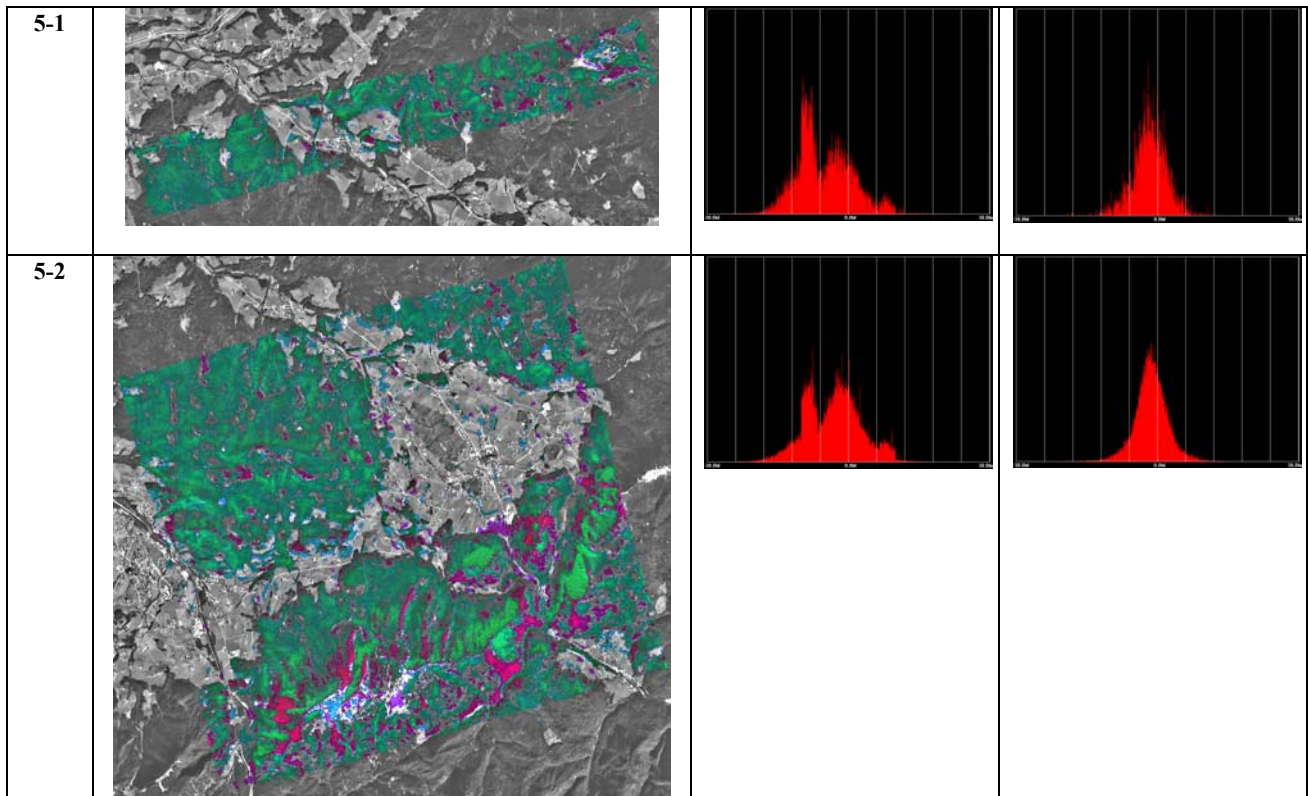


Table 7. Accuracy analysis based on orthogonal distances. In each comparison the absolute maximum distance, the average distance, the standard deviation and the RMSE are shown in meters.

DEM	PROCEDURE 1				PROCEDURE 2			
	Max distance	Average distance	Standard deviation	RMSE	Max distance	Average distance	Standard deviation	RMSE
1	19.60	1.6	1.5	2.2	18.7	2.2	1.7	2.8
2	37.99	1.8	1.8	2.6	37.5	2.7	2.0	3.4
3	22.33	1.4	1.3	1.9	21.4	2.7	1.8	3.2
4	19.74	1.5	1.4	2.1	20.0	2.2	1.6	2.7
5-1	26.25	6.3	4.3	7.6	26.3	6.4	4.4	7.8
5-2	73.60	6.8	5.8	8.9	70.1	6.0	5.0	7.8

## 8. CONCLUSIONS

In this report the methodology applied and the results obtained during the ISPRS-CNES Initiative about DEM generation from SPOT5-HRS are described.

Our Institute was involved as Co-Investigator in the HRS-SAP Initiative through the processing of the dataset number 9, located in Bavaria (Germany).

All the algorithms used to process the data and generate the DSMs have been developed at our Institute. Using the information contained in the image metafile and a suitable number of GCPs, the images have been oriented according to two different approaches, based on a rigorous sensor model for CCD linear array sensors with along-track stereo capability (Procedure 1) and on Rational Polynomial Functions (Procedure 2). More than eight million image points have been measured in the stereopair with the modified Multi Photo Geometrically Constraint matching algorithm designed for pushbroom imagery. Using the two orientations estimated by Procedures 1 and 2, two distinct DSMs of the full area (120km

x 60km) have been generated and compared to the reference DEMs. For the quality control, a 2.5D (calculation of height differences) and 3D analysis (normal distance between one reference surface and the measured DEM) have been used. Also, the areas covered by trees have been manually removed in order to provide a congruent analysis in order to judge the influence of trees.

From both the 2.5D and 3D quality analysis it resulted an average error between the generated and the reference DSMs of around 1-2 pixels (2.5D analysis) and up to slightly more than 1 pixel (3D analysis), depending on the terrain type. The best results were achieved in smooth and flat areas, while in mountain areas some blunders even exceeded 100 meters. The differences between the DSMs obtained by the two different methods of orientation were less than a fourth of a pixel.

In conclusion, the work carried out at ETH confirmed within the HRS-SAP Initiative the high potential of SPOT5-HRS scenes for DEM generation.

## ACKNOWLEDGMENTS

We like to thank Mr. Alain Baudoin, CNES, and Mr. Manfred Schroeder, Chairman of ISPRS Commission I, WG 2 "WG I/2 Sensor Calibration and Testing", for the establishment and coordination of the HRS-SAP Initiative and for accepting our Institute as Co-Investigator.

Thanks also go to DLR Oberpfaffenhofen, and in particular to Dr. Peter Reinartz for providing the ground data (reference DEMs, object points) and for supplying all required information.

## REFERENCES

Baltsavias, E. P., 1991. Multiphoto Geometrically Constrained Matching. Dissertation, IGP, ETH Z, rich, Mitteilungen No. 49, 221 pages.

Baudoin, A., Schroeder, M., Valorge, C., Bernard, M., Rudowski, V., 2003. The HRS-SAP initiative: A scientific assessment of the High Resolution Stereoscopic instrument on board of SPOT 5 by ISPRS investigators. ISPRS Workshop "High resolution mapping from space 2003", October 2003, Hannover, Germany. Proceedings on CD.

CNES site: <http://www.cnes.fr>

DIMAP site: <http://www.spotimage.fr/dimap/spec/dimap.htm>

Dowman, I. J., Michalis, P., 2003. Generic rigorous model for along track stereo satellite sensors. Proceedings of ISPRS Workshop "High Resolution Mapping from Space 2003", Hannover, 4-6 October. Proceedings on CDROM.

Fritsch, D., Stallmann, D., 2000. Rigorous photogrammetric modelling processing of high resolution satellite imagery. International Archives of Photogrammetry and Remote Sensing, Vol. 33, Part B1, Amsterdam, pp.313-321.

Gleyzes, J.-P., Meygret, A., Fratter, C., Panem, C., Baillarin, S., Valorge, C., 2003. SPOT5: System overview and image ground segment. IGARSS 2003, Toulouse, France. Proceedings on CD.

Grodecki, J., and Dial, G., 2003, Block Adjustment of High-Resolution Satellite Images Described by Rational Functions. Photogrammetric Engineering and Remote Sensing, Vol. 69, No. 1, pp. 59-70.

Gruen, A., 1985, Adaptive Least Squares Correlation: A powerful Image Matching Technique. South Africa Journal of Photogrammetry, Remote Sensing and Cartography, 14 (3), pp. 175-187.

Gruen, A., Baltsavias, E. P., 1988, Geometrically Constrained Multiphoto Matching. Photogrammetric Engineering and Remote Sensing, Vol. 54, No. 5, pp. 633-641.

Gruen, A., Zhang L., 2002. Automatic DTM Generation from Three-Line-Scanner (TLS) images. IAPRS, Vol. 34, Part 2A, Graz, Austria, pp. 131-137.

Otto, G. P., Chau, T. K. W., 1988. A Region-Growing Algorithm for Matching of Terrain Images. Proc. 4th Alvey Vision Club, University of Manchester, UK, 31 Aug. - 2 Sept.

Poli, D., 2003. Georeferencing of MOMS-02 and MISR stereoisimages with strict sensor model. ISPRS Workshop "High resolution mapping from space 2003", October 2003, Hannover, Germany. Proceedings on CD.

Tao, C. V., Hu, Y., 2001. A comprehensive study of the rational function model for photogrammetric processing. Photogrammetric Engineering and Remote Sensing, Vol 67, No. 12, pp. 1347-1358.

Zhang L., Gruen, A., 2003. Automatic DSM Generation from StarImager (SI) Data. 6th Conference on Optical 3-D Measurement Techniques September 22-25, 2003 Zurich, Switzerland.

Zhang L., Gruen, A., 2004. Automatic DSM Generation from Linear Array Imagery Data. IAPRS, Vol. 34, Part B3 (to be published).